

Automatic Visual Detection of Incorrect Endoscope Adaptions in Chemical Disinfection Devices

Timo Brune¹, Björn Brune², Sascha Eschborn² and Klaus Brinker¹

¹University of Applied Sciences Hamm Lippstadt, Marker Allee 76-78, Hamm, Germany

²Olympus Surgical Technologies Europe, Kuehnstraße 61, Hamburg, Germany

Keywords: Computer Vision, Feature Detection, Surf, Sift, Registration, Machine Learning, Supervised Learning, Endoscopes, Disinfection.

Abstract: This paper presents a complete analyzing system for detecting incorrect endoscope adaptions prior to the use of chemical disinfection devices to guarantee hygienic standards and to save resources. The adaptions are detected visually with the help of an image registration algorithm based on feature detection algorithms. On top of the processing pipeline, we implemented a k-nearest neighbor algorithm to predict the status of the adaption. The proposed approach shows good results in detecting the adaptions correctly.

1 INTRODUCTION

Endoscopic diagnostic is the main application for diseases of the gastrointestinal tract and has a huge clinical relevance. An important part of endoscopes is the quality of the preprocessing of the devices and the resulting hygiene, to minimize the contamination of the patient with microbes (Bader, 2002). In the past microbes have developed resistances against antibiotics. Consequent hygiene is therefore indispensable. Muscarella (Muscarella, 2014) showed that insufficient preprocessed endoscopes are responsible for the contamination with CRE-microbes. To guarantee an acceptable hygienic standard, we need to disinfect the endoscopes. To do this in a constant quality we apply supervising preprocessing of the endoscopes.

So called cleaning and disinfection devices for endoscopes (CDD-E) perform well in cleaning the endoscope's exterior and interior, where the procedure of adaption is rather complex. Medical employees often do not adapt the endoscopes correctly to the CDD-E because of this complexity. These adaption errors lead to a lack of hygiene. The CDD-E is able to detect these errors and can terminate the process of cleaning. An interruption always costs operational time of up to 20 minutes, water, cleaning chemicals and energy. We have implemented a system tailored to detect those adaption errors prior to the disinfection to save these

resources and ensure the quality of the preprocessing.

We consider the margin between an endoscope adapter and its adaption counterpart in the chemical disinfection device in order to detect connection faults. We have transformed the underlying problem of determining the size of the gap between the respective parts into an image registration problem (Handels, 2009). Hence we want to try to align two reference images of the two sides of the adapter to an image of the disinfection device which contains the endoscope and the adaption counterparts. Please note that this new image is a 2d-projection of the underlying 3d-scene. In this paper we make use of a feature-based approach to image registration (Zitova, 2003). The first step in this processing pipeline is to detect feature points for each image independently. In a second step corresponding feature points on different images are matched.

We detect feature points with two different feature detection algorithms which detect, describe and match possible correspondences and compare their performance on our problem. More precisely we choose the algorithms scale-invariant feature transform (SIFT) (Lowe, 2004) and speeded up robust features (SURF) (Bay, 2008). We describe these feature detection algorithms in more detail in Chapter 2.2.4.

On top of the extracted features we use a simple k-nearest neighbor algorithm to classify correct / incorrect adaptions. More details are given in

Chapter 2.2.5. Finally we show promising experimental results on the accuracy of our automatic error detection prototype in Chapter 3.

2 PROCEDURE

2.1 Hardware Setup

To accomplish the tasks of detecting errors in the adaption, a complete prototype was built. The system consists of a loading station wherein the detection occurs and the integrated software which is responsible for the processing pipeline of the detection. As a basis for our image processing are four images taken by four high-resolution cameras from four different perspectives in order to capture images without occlusions of relevant parts with a high probability. Figure 1 shows an example of an image which was taken by one of the cameras.

For optimal image processing it is important that the scene is illuminated using controlled light conditions (Bader, 2002). Because of that the detection system is sealed in a cube to prevent diffuse light entering the system. We enlighten the detection system with a planar LED-Panel.

Camera sensors take 50% of the information from the green interval of the spectrum. Green light transfers approximately 72% of the luminance and is therefore most important for contrast and resolution (Fukanaga, 1975) Because of that we chose an LED-Panel with a color temperature of 6000 °K. According to Wiens Law, the maximum radiation is at 482.95 nm for 6000 °K which is within the green part of the spectrum.



Figure 1: Example image of the scene, taken by one of the four cameras.

The cameras are controlled using a serial interface from the software to automate the system. With the software we are also able to manipulate the settings

of the camera. So it is possible to adjust the aperture, the ISO-value and the white balance. The white balance is analogically set to 6000 °K. The other values were set empirically, so that there is no over-exposure and therefore no loss of information. We use Canon EOS 750D cameras with a resolution of 24 Megapixel. A high resolution is essential for an accurate detection.



Figure 2: Prototype.

We consider the task of detecting adaption errors for a variety of different endoscopes and adapters. In order to detect which endoscope is used, it is tagged with an RFID chip. We use an RFID-reader, also connected via a serial interface to differentiate between them through their integrated RFID-tags. On the basis of the detected endoscope the software determines which and how many adapters should be connected to the respective endoscope. The user gets visual information on how to attach these adapters to the detected endoscope. Figure 2 shows the general setup of our prototype. At the front there is a door which is not visible in the image.

2.2 Algorithmic Components

In order to classify whether an adapter is connected correctly or not we use a pipeline of algorithms which are explained in more detail in this chapter.

2.2.1 Image Registration

As explained in the introduction, we need to measure the size of the gap between the two sides of the adapter. We took several reference image pairs of each adapter as shown in Figure 3.



Figure 3: left: two parts of the same adapter, right: both adapters matched together show a complete view of the adapter.

If we combine those two parts of the image we get a complete view of the adapter. Our goal is to map and accordingly register these two-dimensional reference images independently on a two dimensional projection of the scene. For image registration, two images are needed. The first is called reference image denoted B_R , and the second is called template image denoted B_T . This leads to a mathematical optimization problem. We search for a linear mapping $t: \mathbb{R}^3 \rightarrow \mathbb{R}^3$ that maps the object on B_R the most exact to the object of B_T . Depending on the class of transformations we can differentiate between rigid, affine and perspective transformation. The positions of the endoscope and thus the adapters are completely unknown and only depend on the employee of the hospital. Therefore, we are not able to reach our goal with a simple rigid or affine transformation. We have to describe a three-dimensional transformation in space as a two-dimensional projection in the image layer (Schreer, 2005). A projection like this is defined as an endomorph description of a scene (Fischer, 2014).

A property of perspective projection is the loss of proportions. Objects that are further away from the center of projection appear smaller.

We can define this transformation as a 3×3 matrix

$$T_P = \begin{pmatrix} \cos \alpha C_x & -\sin \alpha S_v & T_x \\ \sin \alpha S_h & \cos \alpha C_y & T_y \\ P_x & P_y & 1 \end{pmatrix} \quad (1)$$

which we apply to every position of the reference image.

It is now known which form the transformation matrix has to have to map a two-dimensional reference image into the three-dimensional space and map it again to a two-dimensional projection. We have to determine the nine degrees of freedom which uniquely define the matrix. To find the required parameters, we need two sets of corresponding points. A is a set of points from the

reference image and A' is a set of corresponding points from the template image. Here T_P is the transformation matrix of the perspective projection.

$$A \cdot T_P = A' \Leftrightarrow T_P = A^{-1}A' \quad (2)$$

To determine the transformation matrix we need to have correspondences of points in the reference and template image. In the following chapter we show how these correspondences are detected.

2.2.2 Feature Detection

Feature detection algorithms are methods from the field of computer vision. We use them to detect so called interest points and correspondences between points in two images. These images typically show the same object, but at a different time or from a different perspective. In the experiments we will analyze two well established algorithms to examine which one is more appropriate for this application field. The two algorithms are the scale-invariant feature transform (SIFT) (Lowe, 2004) and the speeded up robust features (SURF) (Bay, 2008). These two algorithms have the same general process, which is divided into three steps: 1. feature detection, 2. feature description and 3. feature matching.

The first step, feature detection, deals with the detection of so-called interest points. These are distinctive points in an image. They always depend on their neighborhood.

The feature description deals with the description of the detected interest points, enabling a comparison between the reference and the template images. The most significant feature is the surrounding of one point. Since the surroundings of the interest points are never exactly the same on the reference and the template image, a pixelwise comparison would not work robustly. Furthermore, the descriptors have to be invariant against geometric, perspective and illumination transformations and image noise. Both algorithms are based on computing one gradient of the complete neighborhood of an interest point, as well as in their sub regions.

The final step of the feature detection algorithms matches interest points in the reference and template image. The challenge is to find correct correspondences of points, which in fact show the same points of an object (Szeliski, 2011).

Every interest point is described through a multidimensional description vector. A similarity can be evaluated with the Euclidean distance between the two descriptors. The most accurate but slowest method is to compare every interest point of

the reference image with every interest point of the template image. Since accuracy is one of our main goals, we make use of this algorithm in the experimental section. Other possibilities are the randomized k-d tree (Silpa-Anan, 2008) and the priority k-means tree algorithm (Fukanaga, 1975). These algorithms are up to two times faster, approximate to 95% of correctness (Muja, 2014).

Despite the high accuracy of SIFT and SURF, there are always a few correspondence errors which have to be filtered. We filter these errors with the well-established random sample consensus algorithm (RANSAC) (Strutz, 2016). If these errors were not filtered they would have a bad influence on the computation of the transformation matrix.

2.2.3 Machine Learning

To classify if an adapter is adapted correctly we use a simple k-nearest neighbor approach. As features we use the Euclidean distance between the two projections and the number of detected correspondences. Figure 4 shows an example of registered features on one of the adapters. In this example the classes are linear separable.

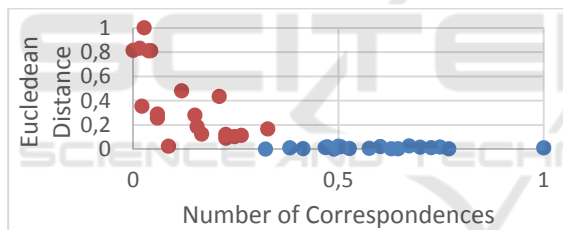


Figure 4: Normalized values of the Euclidean distances and the number of correspondences, red: incorrect, blue: correct.

2.2.4 Processing Pipeline

In this section we explain the complete processing pipeline. Figure 5 shows four template images made at runtime as explained previously.

We take five reference image pairs for every adapter. One part of the pair shows the part of the adapter at the endoscope, the other one the part of the tube. The process is the same for every adapter.

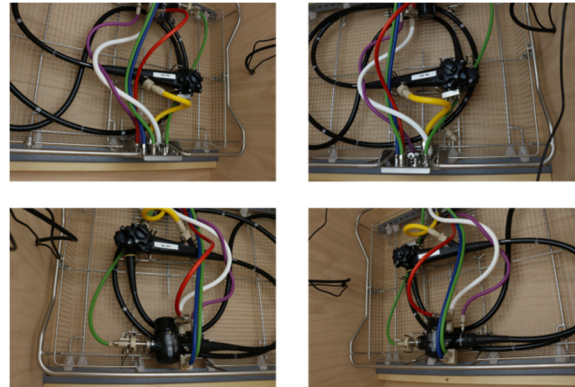


Figure 5: Template images from four different perspectives.

At first we intend to find the rough position of the endoscope. For this purpose we use the feature detection algorithm to find correspondences between a reference image of the part of the adapter at the endoscope.



Figure 6: Correspondence pairs between the reference image and the template image to detect the rough position of the adapter.

These interest points and correspondences are easier to find because of the texts on the endoscope which are very distinctive. We compute the mean of all detected points in Figure 6 and crop that region of the image depending on the size and geometry of the adapter. This happens at a fourth of the resolution to save time. The following computations are made on the cropped images. This approach has two advantages. First: The complex computations are made on a much smaller image. Second: A smaller image minimizes the probability of correspondence errors.

When all subregions for all adapters were found, the accurate registration of the reference image pairs begins. For every adapter we have five reference image pairs. As one can see in Figure 7 the adapters not only have to be transformed in the space but may have to be rotated longitudinally as well. For the accurate registration we check all reference images and choose the one with the most detected

correspondences.

Afterwards we detect and describe the interest points of the chosen reference image of the adapter on the side of the endoscope and the associated reference image of the adapter on the side of the tube. Then we identify correspondences between the reference images and compute the transformation matrices as shown in equations (1) and (2). With the computed transformation matrices we map the reference images into the template image we identified previously. If the adaption is correct, the projected reference images should intersect on the inner edge as pictured in Figure 3. The same matrices for mapping the reference images are used to compute the center of the cutting edge. In Figure 8 one can see the two mapped reference images, bounded in green rectangles. The midpoints of the cutting edges are depicted by blue points. One can recognize only one point at the left image because of the optimal projections the two points overlap completely. In the right image one can see an incorrect adaption. The Euclidean distance between the points is one feature for the classification of the incorrect adaption.



Figure 7: A variety of reference images of the same adapter because of the longitudinal rotations, which are not detectable with the feature detection algorithms.

We use the two points to compute the Euclidean distance between the two projections. An explorative data analysis showed that the projection does not work perfectly at all times. So it is not reliable as single. Because of that we implemented a simple k-nearest-neighbor Algorithm to classify the adaptions. In addition to the Euclidean distance we use the number of correspondences as a second feature. This is depicted in Figure 4.

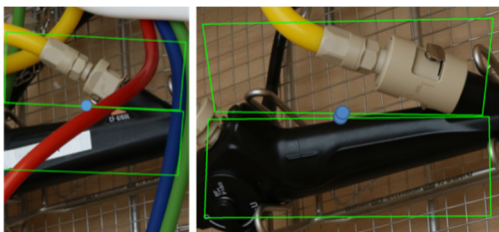


Figure 8: Mapped reference image pair on one template image. The blue point marks the middle of their cutting edges. Left: correct adaption, right: incorrect adaption.

3 EXPERIMENTAL RESULTS

As stated in the previous chapter, the detection of interest points and correspondences is essential for a correct projection of the reference images. The quality of the transformation matrix is significantly enhanced by detecting more correspondences. Vice versa a faultless projection is impossible if there are too many correspondence errors. In this chapter we describe the results of the detection processes and of the classification.

We describe only the results of the reference images on the side of the adapter. Because of the high amount of letters on the endoscope itself, there are a lot of interest points and the projection always worked faultless.



Figure 9: Adapter set which we used for our experiments.

The quantitative results of the feature detection algorithms are our first criteria for the quality of the system. Figure 9 shows the adapter set we used for our experiments. In the following tables we show the statistic results of 40 processes for the first adapter set. Table 1 shows the results for correct adaptions generated with SURF.

The number of interest points and correspondences - absolute and per pixel - is of special importance here. In both categories one can see, that the values are in the same order of magnitude for most adapters. The adapters a, c, f and g have the lowest values. This is because of the little body and the few distinctive points on the adapters. So a correct correspondence is more difficult to compute. The adapters b, d and e have more distinctive points. So the correspondences are easier to find. In Table 2 we see the statistical values for incorrect adaptions, generated with SURF. The number of detected interest points is similar. This makes sense, because we use for both procedures images of the same size. One can see the difference at the inspection of the correspondences. For incorrectly adapted devices the algorithm detects much less correspondences. This is because the reference images were made with correct adaptions.

Table 1: Correct adaptions, generated with SURF as pre-processor.

Adapter	Interest Points			Correspondences				
	Mean #	Minimum #	Maximum #	Mean #	Minimum #	Maximum #	Per Pixel	
a	824 ±90	764	995	3.4 E-3 ±25	139	105	189	5.8 E-4
b	367 ±24	331	382	2.1 E-3 ±12	97	81	115	5.0 E-4
c	349 ±8	339	357	1.0 E-3 ±13	52	23	65	1.6 E-4
d	572 ±12	561	586	1.9 E-3 ±6	53	45	63	1.7 E-4
e	107 ±3	106	117	1.9 E-3 ±10	17	9	43	3.0 E-5
f	111 6 ±82	883	114 2	3.4 E-3 ±21	142	114	114	4.0 E-4
g	441 ±33	371	465	2.0 E-3 ±6	26	18	35	1.1 E-4

Table 2: Incorrect adaptions, generated with SURF as pre-processor.

Adapter	Interest Points			Correspondences				
	Mean #	Minimum #	Maximum #	Mean #	Minimum #	Maximum #	Per Pixel	
a	794 ±33	780	888	3.3 E-3 ±16	38	24	73	1.6 E-4
b	356 ±26	323	382	2.0 E-3 ±5	15	10	25	8.0 E-5
c	342 ±6	339	354	1.0 E-3 ±2	7	5	10	2.0 E-5
d	566 ±29	540	602	1.8 E-3 ±9	19	12	40	6.0 E-5
e	159 ±58	106	227	2.8 E-3 ±38	35	4	86	6.0 E-5
f	873 ±310	142	114 2	3.0 E-3 ±27	60	27	91	1.8 E-4
g	424 ±49	324	465	1.9 E-3 ±4	9	7	19	4.0 E-5

If there is an incorrect adaption in the template image it is possible, that there are large perspective changes. If the perspective changes are too high, the SURF algorithm cannot detect them, so fewer correspondences are found as one can see in Figure 10. In six of the seven cases there are more than twice as many detected correspondences. The only exception here is adapter g because of its simple structure and few interest points. These experimental evaluations demonstrate that the number of correspondences is a meaningful feature for the machine learning algorithm.

Table 3: Correct adaptions, generated with SIFT as pre-processor.

Adapter	Interest Points			Correspondences				
	Mean #	Minimum #	Maximum #	Mean #	Minimum #	Maximum #	Per Pixel	
a	402 ±5	391	407	1.7 E-3 ±13	80	54	91	3.3 E-4
b	135 ±8	121	140	8.0 E-4 ±5	46	38	51	2.6 E-4
c	157 ±13	140	170	5.0 E-4 ±5	14	7	26	1.0 E-5
d	321 ±20	278	336	1.0 E-3 ±7	23	15	33	7.0 E-5
e	52 ±8	41	58	9.0 E-4 ±3	9	5	13	1.5 E-4
f	697 ±185	206	776	2.0 E-3 ±10	208	191	220	6.3 E-4
g	238 ±40	199	339	1.0 E-3 ±5	17	10	28	7.0 E-5

In the following we outline the results of SIFT for the same adapter set. The statistical values of correct adaptions are shown in Table 3. Compared to the SURF algorithm it attracts attention that SIFT detects less interest points and correspondences than SURF. The exact quotient is shown in Figure 11. One can easily see that the SURF algorithm detects more interest points and because of that more Correspondences.

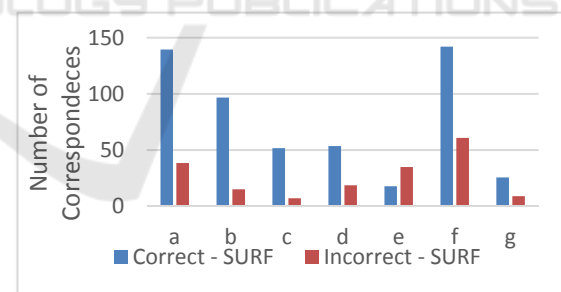


Figure 10: Comparison of the number of correspondences between correct and incorrect adaptions.

In Table 5 one can see the statistical values for incorrect adaptions, generated with SIFT. Analogue to the SURF algorithm it is obvious that fewer correspondences have been computed. This is because of the similar procedure. Striking are the detected minima of correspondences. If the algorithm detects less than three correspondences, a projection and following classification is impossible. In summary we conclude, that the SURF algorithm detects roughly twice as many correspondences than

the SIFT algorithm. If we have too few correspondences it is possible that the RANSAC algorithm cannot filter the correspondence errors. The result is an incorrect transformation matrix. Quantitatively the SURF algorithm has to be preferred.

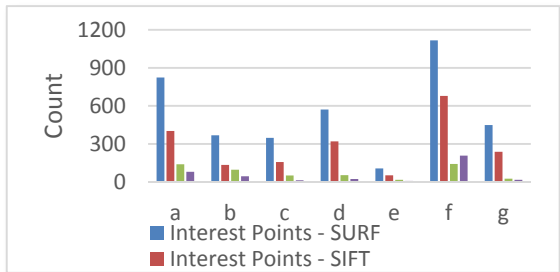


Figure 11: Comparison of the detected interest points and correspondences.

Now we will focus on the quality and precision of the classification. As outlined before we use a k-nearest neighbor Algorithm for the binary classification. The Euclidean distance of the projection pairs and the number of correspondences are the features of the algorithm. Experiments with validation data gave us an optimal value for $k = 5$.

A first estimation of the quality of the processes delivers the classification rate. In Figure 12 one can see the classification rate per adapter for both algorithms as pre-processing. All rates were determined on test data experiments.

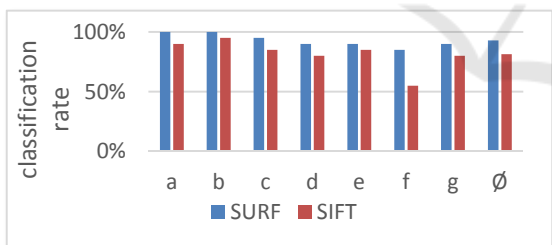


Figure 12: Comparison of the classification rates.

As predicted the process with SURF as pre-processing has a significantly higher classification rate of 92.86% compared to SIFT. The worst value occurs at adapter e. This is because of the geometry of the adapter. The Euclidean distance can be 0 for this adapter although it is adapted incorrectly. This adapter needs an additional physical rotation to be correctly adapted. This can only be determined through the number of detected correspondences.

Table 4: Confusion matrix of the classifications with SURF as pre-processing.

SURF	CORRECT ADAPPTIONS	INCORRECT ADAPPTIONS	
PREDICTED CORRECT ADAPPTIONS	TP = 64	FP = 4	$P' = 68$
PREDICTED INCORRECT ADAPPTIONS	FN = 6	TN = 66	$N' = 72$
	$P = 70$	$N = 70$	$\Sigma = 140$

Fawcett explains another possibility to evaluate classifications (Fawcett, 2006). So called receiver operating characteristics (ROC) graphs can be used to evaluate and visualize the quality of a classification. We divide the results of our experiments in four groups: true-positive (TP), true-negative (TN), false-positive (FP) and false-negative (FN). These groups can be written in a so-called confusion matrix (Fawcett, 2006), as one can see in Table 4 and Table 6.

Table 5: Incorrect adaptations, generated with SIFT as pre-processor.

Adapter	Interest Points				Correspondences			
	Mean #	Minimum #	Maximum #	Per Pixel	Mean #	Minimum #	Maximum #	Per Pixel
a	339 ±5	397	409	1.7 E-3	40 ±9	24	51	1.6 E-4
b	136 ±7	121	140	8.0 E-4	10 ±6	3	19	5.0 E-5
c	160 ±35	140	256	5.0 E-4	5 ±2	3	8	1.0 E-5
d	317 ±21	278	336	1.0 E-3	18 ±6	9	30	5.0 E-5
e	131 ±99	41	246	2.3 E-3	26 ±25	3	76	4.6 E-4
f	711 ±105	557	776	2.2 E-3	142 ±53	44	209	4.3 E-4
g	203 ±14	190	239	9.0 E-4	8 ±3	4	13	3.0 E-5

The contents of the matrices were generated in 40 experiments and are a summary of all adapters. P is the number of correct, N is the number of incorrect adaptations. P' is the number of positive, N' is the number of negative predictions. We can derive four statistical values from these matrices: the true-positive-rate (TPR), the false-positive-rate (FPR), positive-predictive-value (PPV) and the accuracy (ACC). We can now visualize the quality of the classification with a ROC-Graph as shown in Figure 13.

Table 6: Confusion matrix of the classifications with SIFT as pre-processing.

SIFT	CORRECT ADAPPTIONS	INCORRECT ADAPPTIONS	
PREDICTED CORRECT ADAPPTIONS	TP = 62	FP = 18	P' = 80
PREDICTED INCORRECT ADAPPTIONS	FN = 8	TN = 52	N' = 60
	P = 70	N = 70	$\Sigma = 140$

Ideally should the TPR be close to 1, the FPR close to 0. The more the point is in the North-West, the better is the classification. One can see in the visualization that the processes with SURF as Pre-Processing Algorithm is better than with SIFT. The system needed in average 71/42 seconds for the classification of the large/small adapter set.

Table 7: Statistical values from the confusion matrices.

	SURF	SIFT
TPR	0.914	0.886
FPR	0.057	0.257
PPV	0.941	0.775
ACC	0.928	0.814

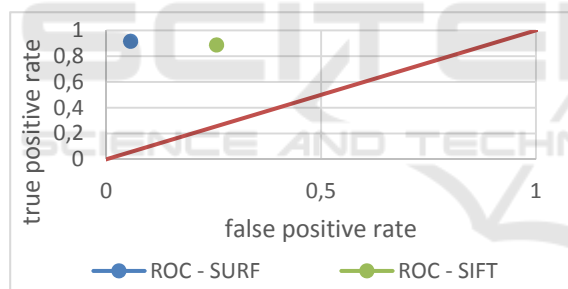


Figure 13: ROC Graph.

4 CONCLUSION

This paper presents an automatic visual system for detecting adaption errors in chemical disinfection devices for endoscopes. Our experimental evaluation shows promising results with respect to the classification accuracy. With the SURF algorithm as pre-processing tool, the prototype system yields a classification accuracy of 92.86% for determining the correctness of the adaptations in approximately one minute of processing. Future work will aim in enhancing the correctness of the prediction close to 100% and in installing the system directly into the endoscope thermal disinfector to save even more time and resources.

REFERENCES

- Bader, L. et al, 2002 HYGEA (Hygiene in Gastroenterology – Endoscope Reprocessing): Study on Quality of Reprocessing Flexible Endoscopes in Hospitals or Practice Setting. In *Journal for Gastroenterology 12 Pages 951-1000*.
- Muscarella, L., 2014 Risk of transmission of carbapenem-resistant Enterobacteriaceae and related “superbugs” during gastrointestinal endoscopy. In *World Journal of Gastrointestinal Endoscopy 6 Pages 951-1000*.
- Handels, H., 2009. Medizinische Bildverarbeitung, Vieweg und Teubner. Wiesbaden, 2nd edition.
- Zitova, B., Flusser, J., 2003. Image registration methods: a survey. In *Image and Vision Computing Volume 21 Pages 977-1000*.
- Lowe, D., 2004, Distinctive Image features from Scale-Invariant Keypoints. In *International Journal of Computer Vision 60 Pages 91-110*.
- Bay, H. et al, 2008, Speeded-Up Robust Features (SURF). In *Computer Vision and Image Understanding Pages 346-359*.
- Schreer, O., 2005. Stereoanalyse und Bildsynthese, Springer Verlag. Berlin Heidelberg, 1st edition.
- Fischer, G., 2014. Lineare Algebra, Springer Verlag. Berlin Heidelberg, 18th edition.
- Szeliski, R., 2011. Computer Vision, Springer Verlag. Berlin Heidelberg, 1st edition.
- Silpa-Anan, C., Hartley, 2008, R., Optimised KD-Tree for fast image descriptor matching. In *Computer Vision and Pattern Recognition*
- Fukanaga, K., Narendra, P., 1975, A branch and bound Algorithm for Computing k-Nearest Neighbors. In *IEEE Transactions on Computers C-24 Pages 750-753*.
- Muja, M., Lowe, D., 2014, Scalable Nearest Neighbor Algorithms for High Dimensional Data. In *IEEE Transactions on Pattern Analysis and Machine Intelligence 36 Pages 2227-2240*.
- Strutz, T., 2016. Data Fitting and Uncertainty, Springer Verlag. Berlin Heidelberg, 2nd edition.
- Fawcett, T., 2006, An introduction to ROC Analysis. In *Pattern Recognition Letters 27 Pages 861-874*.